Supplemental: Ab-initio Calculations of Vibrational Fingerprints in the Photoluminescence of Graphene Quantum Dots

Ruoyu Wu,[1] Peng Han,[1,*] Tobias Dittmann,[2] Fuhe Wang,[1] Yan Zhang,[1] and Gabriel Bester[2,3,†]

[1] *Department of Physics, Beijing Key Lab for Metamaterials and Devices, Capital Normal University, Beijing 100048, China*
[2] *Departments of Chemistry and Physics, Universität Hamburg, Luruper Chaussee 149, D-22761 Hamburg, Germany*
[3] *The Hamburg Centre for Ultrafast Imaging, Luruper Chaussee 149, D-22761 Hamburg, Germany*

(Dated: October 28, 2024)

In this supplementary document, we supply information concerning the geometry and electronic structures of all the graphene quantum dots (GQDs) studied in the paper, the characters of nine dominated Huang-Rhys (HR) active vibrational modes of GQDs, and explain the videos of these HR active modes in GQDs with various geometry structures and edge orientation. Moreover, the photoluminescence (PL) spectrum of hex-zig GQDs with L =19.6 Å and 29.4 Å along with the separately plotted exciton-induced atomic displacements for GQDs with different geometry and edge structures are also presented.

I. GEOMETRY STRUCTURES OF GQDS

In Fig. S1, we present the geometry structures of all the GQDs we studied in the paper. The carbon and hydrogen atoms are presented as cyan and white spheres, respectively. The atomic structures along with the keywords "hex", "tri", and "arm", which have been defined in the paper, are given above the geometry structures.

II. ELECTRONIC STRUCTURES OF GQDS

In Fig. S2, we present the calculated electronic structures of all the GQDs we studied in the paper within the framework of local density approximation and Trouiller-Martin normconserving pseudopotentials. The occupied and un-occupied electronic states are plotted as solid red and blue lines, respectively. The degeneracy of electronic states beyond one-folded obtained from our density functional theory calculation (DFT) calculation is presented around the energy level. To understand the effect of symmetry on the degeneracy of electronic states, we labeled the point group symmetry for each GQD obtained from density functional theory calculation.

*E-mail:peng.han@cnu.edu.cn
†E-mail:gabriel.bester@uni-hamburg.de

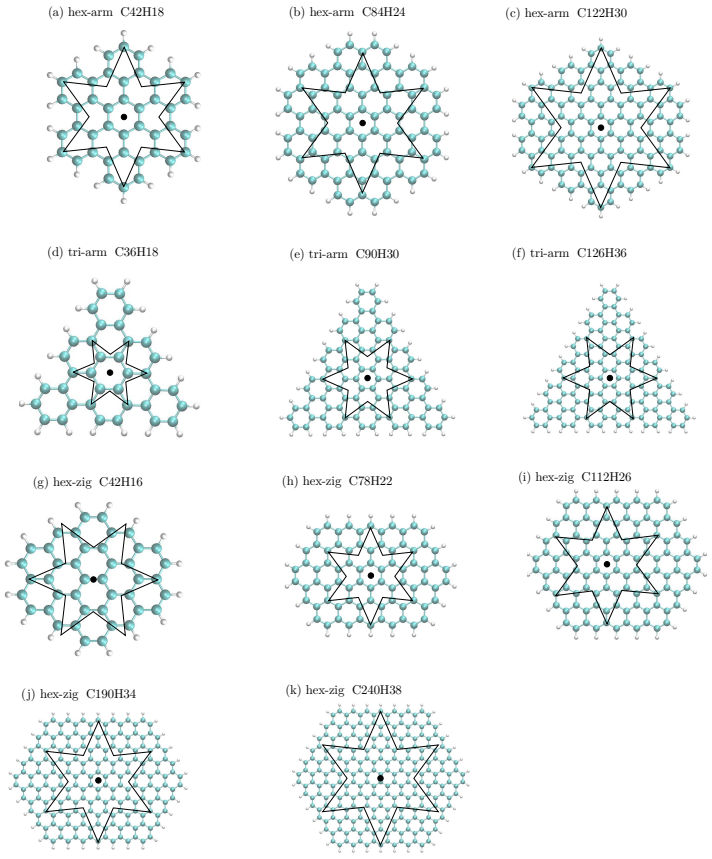

FIG. S1: Geometry structures of GQDs we studied in this work along with their atomic structures. The names given above the structures are used as the keywords throughout the paper.

III. CHARACTERS OF NINE DOMINATED HR ACTIVE MODES

In Table II of the main paper, we present nine dominant HR active modes of hexagonal GQDs with zigzag and armchair edge structures and triangle GQDs with armchair edges along with their origination. In the follows, we list the characters of these modes with detailed descriptions in Table S1.

TABLE S1: Nine dominant HR active vibrational modes of hexagonal (hex) and triangular (tri) GQDs with zigzag (zig) and armchair (arm) edge structures.

Mode	GQDs	character	remark
1	tri-arm	oblate-prolate, but distorted because of the triangular	oblate-prolate mode
2		ring breathing mode	ring breathing mode
3		rings get to square, like in mode 5 but in the entire structure	ring-to-square mode
4	hex-arm	oblate-prolate	oblate-prolate mode
5		ring-breathing mode	ring breathing mode
6		ring get to square, but in entire structure	ring-to-square mode
		but in entire structure	
7	hex-zig	oblate-prolate vibration	oblate-prolate mode
8		ring-breathing mode, longitudinal optical	ring breathing mode
9		only rings in the middle [001] plane move, the rings get to squares,	ring-to-square mode
		4 atoms out of 6 move, transverse optical	

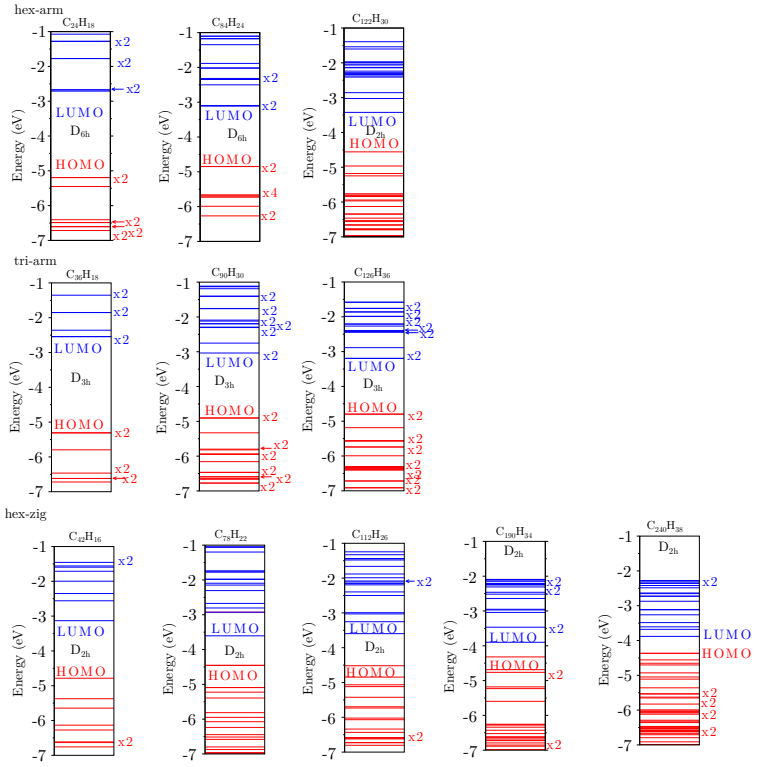

FIG. S2: Electronic structures of GQDs we studied in this work along with their atomic structures and the corresponding point group symmetry. The occupied and un-occupied electronic states are presented as red and blue lines, respectively. The degeneracy of electronic states beyond one-folded is presented.

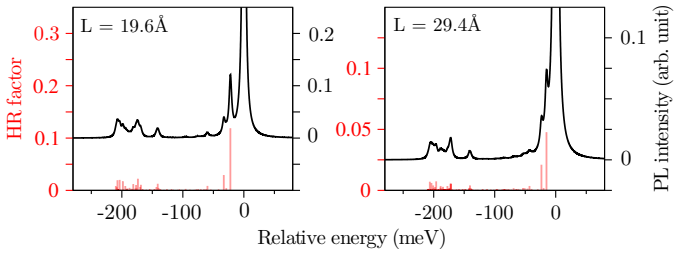

FIG. S3: Calculated PL intensity (black lines) including only class 1 transitions and HR factors (red bars) for hex-zig GQDs with sizes of L =19.6 Å and 29.4 Å . The ZPL is shifted to zero relative energy and is normalized to one.

IV. PL SPECTRUM OF HEX-ZIG GQDS WITH L =19.6 Å AND 29.4 Å

In Fig. S3, we present the calculated PL spectrum of hex-zig GQDs with sizes of L =19.6 Å and 29.4 Å using a broadening of 2 meV as solid black lines. The calculated HR factors are presented as solid red bars in Fig. S3. To focuse on the phonon sidebands of PL spectrum, we plot the PL spectrum as a function of the relative energy to the zero phonon line (ZPL) and normalized the intensity of ZPL to one.

V. LATTICE DISPLACEMENT VS. DISTANCE TO GQD CENTER

In Fig. S4, we separately plot the calculated exciton-induced atomic displacements as a function of distance to the GQD center for GQDs with different geometry and edge structures.

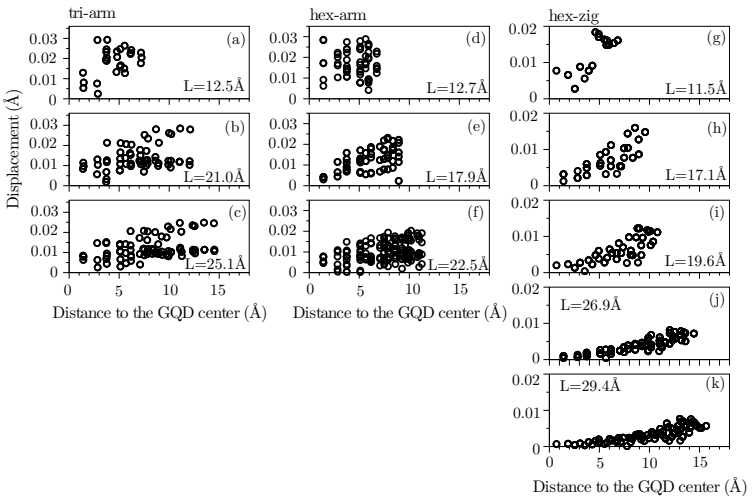

FIG. S4: Exciton-induced atomic displacements as a function of distance to the GQD center for GQDs with different geometry and edge structures.

VI. VISUALIZATION OF HR ACITVE VIBRATIONAL MODES IN GQDS

In the supplementary material part of the submission, we present illustrative movies of the confined acoustic modes, the coherent acoustic modes and in-plane vibrated acoustic modes of GQDs with various sizes, geometry shapes and edge structures. The details of the video files are given in Table S2.

TABLE S2: Videos of vibration

File name	Mode	GQD shape and edge	atomic structure	size L (Å)	Frequency (cm^{-1})
mode1-trzarmL13A.mp4	oblate-prolate mode				294.54
mode2-trzarmL13A.mp4	ring breathing mode	tri-arm	$C_{36}H_{18}$	12.5	1416.86
mode3-trzarmL13A.mp4	ring-to-square mode				1673.11
mode1-trzarmL21A.mp4	oblate-prolate mode				189.54
mode2-trzarmL21A.mp4	ring breathing mode	tri-arm	$C_{90}H_{30}$	21.0	1398.82
mode3-trzarmL21A.mp4	ring-to-square mode				1668.00
mode1-trzarmL25A.mp4	oblate-prolate mode				163.26
mode2-trzarmL25A.mp4	ring breathing mode	tri-arm	$C_{126}H_{36}$	25.1	1391.86
mode3-trzarmL25A.mp4	ring-to-square mode				1666.11
mode4-hexarmL13A.mp4	oblate-prolate mode				277.08
mode5-hexarmL13A.mp4	ring breathing mode	hex-arm	$C_{42}H_{18}$	12.8	1311.18
mode6-hexarmL13A.mp4	ring-to-square mode				1667.24
mode4-hexarmL18A.mp4	oblate-prolate mode				202.68
mode5-hexarmL18A.mp4	ring breathing mode	hex-arm	$C_{84}H_{24}$	17.9	1404.55
mode6-hexarmL18A.mp4	ring-to-square mode				1672.09
mode4-hexarmL23A.mp4	oblate-prolate mode				165.27
mode5-hexarmL23A.mp4	ring breathing mode	hex-arm	$C_{122}H_{30}$	22.5	1390.05
mode6-hexarmL23A.mp4	ring-to-square mode				1668.74
mode7-hexzigL12A.mp4	oblate-prolate mode				272.13
mode8-hexzigL12A.mp4	ring breathing mode	hex-zig	$C_{42}H_{16}$	11.5	1423.04
mode9-hexzigL12A.mp4	ring-to-square mode				1690.80
mode7-hexzigL17A.mp4	oblate-prolate mode				204.57
mode8-hexzigL17A.mp4	ring breathing mode	hex-zig	$C_{78}H_{22}$	17.1	1424.15
mode9-hexzigL17A.mp4	ring-to-square mode				1688.17
mode7-hexzigL20A.mp4	oblate-prolate mode				177.93
mode8-hexzigL20A.mp4	ring breathing mode	hex-zig	$C_{112}H_{26}$	19.6	1423.83
mode9-hexzigL20A.mp4	ring-to-square mode				1692.45
mode7-hexzigL27A.mp4	oblate-prolate mode				136.43
mode8-hexzigL27A.mp4	ring breathing mode	hex-zig	$C_{190}H_{34}$	26.9	1423.78
mode9-hexzigL27A.mp4	ring-to-square mode				1689.63
mode7-hexzigL29A.mp4	oblate-prolate mode				122.37
mode8-hexzigL29A.mp4	ring breathing mode	hex-zig	$C_{240}H_{38}$	29.4	1423.74
mode9-hexzigL29A.mp4	ring-to-square mode				1691.41
mode-E1.mp4	oblate-prolate mode				181.20
mode-E2.mp4	oblate-prolate mode				182.75
mode-E3.mp4	ring breathing mode				1270.42
mode-E4.mp4	ring breathing mode	tri-arm	$C_{96}H_{30}$	18.2	1315.81
mode-E5.mp4	ring breathing mode				1348.25
mode-E6.mp4	ring-to-square mode				1582.90
mode-E7.mp4	ring-to-square mode				1597.79
mode-E8.mp4	ring-to-square mode				1612.53

[S1] H. Raza, Edge and passivation effects in armchair graphene nanoribbons Phys. Rev. B, **84**, 165425 (2011).